



Quantitative transport mapping (QTM) for differentiating benign and malignant breast lesion: Comparison with traditional kinetics modeling and semi-quantitative enhancement curve characteristics.

Qihao Zhang ^{a,b}, Pascal Spincemaille ^a, Michele Drotman ^a, Christine Chen ^a, Sarah Eskreis-Winkler ^a, Weiyuan Huang ^a, Liangdong Zhou ^a, John Morgan ^a, Thanh D. Nguyen ^a, Martin R. Prince ^a, Yi Wang ^{a,b,*}

^a Department of Radiology, Weill Medical College of Cornell University, New York, NY, United States of America

^b Meinig School of Biomedical Engineering, Cornell University, Ithaca, NY, United States of America

ARTICLE INFO

Keywords:

Breast tumor diagnosis
Fluid flow velocity
Dynamic contrast enhanced (DCE) MRI
Arterial input function (AIF)
Quantitative Transport Mapping (QTM)

ABSTRACT

Purpose: To test the feasibility of using quantitative transport mapping (QTM) method, which is based on the inversion of transport equation using spatial deconvolution without any arterial input function, for automatically postprocessing dynamic contrast enhanced MRI (DCE-MRI) to differentiate malignant and benign breast tumors.

Materials and methods: Breast DCE-MRI data with biopsy confirmed malignant ($n = 13$) and benign tumors ($n = 13$) was used to assess QTM velocity ($|u|$) and diffusion coefficient (D), volume transfer constant (K^{trans}), volume fraction of extravascular extracellular space (V_e) from kinetics method, and traditional enhancement curve characteristics (ECC: amplitude A, wash-in rate α , wash-out rate β). A Mann-Whitney U test and receiver operating characteristic curve (ROC) analysis were performed to assess the diagnostic performance of these parameters for distinguishing between benign and malignant tumors.

Results: Between malignant and benign tumors, there was a significant difference in $|u|$ and K^{trans} , ($p = 0.0066$, 0.0274, respectively), but not in D, V_e , A, α and β ($p = 0.1119$, 0.2382, 0.4418, 0.2592 and 0.9591, respectively). ROC area-under-the-curve was 0.82, 0.75 (95% confidence level 0.60–0.95, 0.51–0.90) for $|u|$ and K^{trans} , respectively.

Conclusion: QTM postprocesses DCE-MRI automatically through deconvolution in space and time to solve the inverse problem of the transport equation. Comparing with traditional kinetics method and ECC, QTM method showed better diagnostic accuracy in differentiating benign from malignant breast tumors in this study.

1. Introduction

Perfusion quantification is based on modeling a tracer transport through tissue captured in time-resolved imaging, such as dynamic contrast enhanced (DCE) MRI, and allows quantitative measurements of vascularity associated with tissue pathophysiology and is highly desired in clinical practice. Traditional tracer kinetics modeling has been used for perfusion quantification, which is based on Kety's eq. [1] with Tofts' generalization [2] by relating the temporal change in tracer concentration to an arterial input function (AIF) for each voxel. Since AIF at each voxel is not measurable in practice, a single global AIF is assumed to supply all voxels, which is known to have errors associated with

voxel-level deviations from the global AIF [3]. A voxel specific AIF delay to each voxel may be estimated as an additional parameter in fitting DCE-MRI data [4–6], but estimating AIF dispersion at each voxel is very challenging [3,4,7]. Perfusion quantification from DCE-MRI in practice varies substantially depending on how AIF is obtained [8–10]: a manual selection is operator dependent [3,9,11] while automated methods dependent on a variety of assumptions [12,13]. Consequently, AIF remains an unsolved problem for traditional tracer kinetics approach [3], and current BI-RADS and PI-RADS instead use semi-quantitative temporal characterization of enhancement curves to analyze tumor regions of interest [14,15].

To address the AIF problem in the traditional kinetics modeling of

Abbreviations: DCE, Dynamic contrast enhanced; AIF, Arterial input function; QTM, Quantitative Transport Mapping.

* Corresponding author at: Department of Radiology, Weill Cornell Medicine, 407 East 61st St, Suite RR124, New York, NY 10065, United States of America.

E-mail address: yw233@cornell.edu (Y. Wang).

<https://doi.org/10.1016/j.mri.2021.10.039>

Received 4 April 2021; Received in revised form 29 October 2021; Accepted 30 October 2021

Available online 6 November 2021

0730-725X/© 2021 Elsevier Inc. All rights reserved.

Table 1
Patient information in our study.

	Benign cases	Malignant cases
Age	51.23 ± 13.00 yrs	63.38 ± 11.14 yrs
Lesion size(largest diameter)	1.57 ± 1.39 cm	1.20 ± 0.45 cm
Histopathology	13 benign	5 DCIS; 4 IDC; 1 invasive ductal carcinoma; 1 invasive lobular carcinoma; 1 invasive tubular carcinoma; 1 microinvasive mammary carcinoma
Lesion Type	8 NME; 4 mass; 1 focus	2 NME; 7 mass; 2 focus
Initial BIRADS	8 grade 4; 2 grade 4A; 3 grade 4B	2 grade 4; 1 grade 4A; 3 grade 4B; 2 grade 4C; 5 grade 5;

tracer kinetics, recently a new method has been proposed to model the contrast agent concentration change in space and time according to the transport equation which obtains spatial and temporal derivatives of the concentration and do not require the selection of an AIF [16]. A blood flow velocity can be calculated by inverting the transport equation in a fully automated manner [17,18], which is termed as quantitative transport mapping (QTM) [19,20], in a fully automated manner without any AIF input. Using computational fluid mechanics simulation to validate quantitative tissue perfusion, QTM is shown to be substantially more accurate than traditional kinetics approach for kidney perfusion quantification from time-resolved (multi-delay) 3D arterial spin labeling MRI data [20].

In this work, we investigate the use of QTM for postprocessing time-resolved 3D dynamic contrast enhanced (DCE) MRI of breast tumors and

compare QTM with traditional kinetics method and enhancement curve characterization (ECC). The lack of well-established breast tumor vasculature makes it difficult to use computational fluid mechanics simulation for quantitative perfusion validation. Instead, breast biopsy pathology in characterizing tumor malignancy is available in clinical practice and can be used to evaluate the performances of various quantitative perfusion postprocessing methods in differentiating benign from malignant breast tumors. Accordingly, we report here the diagnostic performance of QTM, traditional kinetics method and ECC for assessing breast tumor malignancy.

2. Methods

2.1. QTM, traditional kinetics method and enhancement curve for postprocessing DCE MRI

In quantitative transport mapping, tracer concentration profile is modeled by a transport equation [16,20]:

$$-\nabla \cdot \mathbf{c}(\mathbf{r}, t)\mathbf{u}(\mathbf{r}) + \nabla \cdot \mathbf{D}(\mathbf{r})\nabla \mathbf{c}(\mathbf{r}, t) = \partial_t \mathbf{c}(\mathbf{r}, t). \quad (1)$$

Here ∂_t is the time derivative, $\nabla = (\partial_x, \partial_y, \partial_z)$ the gradient operator, $\mathbf{c}(\mathbf{r}, t)$ the tracer concentration scalar field at a voxel with index $\mathbf{r} = (r_x, r_y, r_z)$ in a volume of (N_x, N_y, N_z) resolution along (x, y, z) axis, and time index $t \in \{1, 2, \dots, N_t - 1\}$ the time index with N_t as the number of time frames. $\mathbf{u}(\mathbf{r}) = (u^x(\mathbf{r}), u^y(\mathbf{r}), u^z(\mathbf{r}))$ is an average velocity vector field, and $\mathbf{D}(\mathbf{r})$ the diffusion coefficient scalar field [16]. Both time derivative and gradient operator are difference operations in the discretized 4D spacetime-resolved image space. Eq. 1 is a linear equation system for velocity and diffusion that is solved as an optimization problem with L1 total variation regularization as in a recent QTM study with the regularization parameters $\lambda = 10^{-3}$ and $\mu = 10^{-5}$ chosen according to the L-curve method [20]:

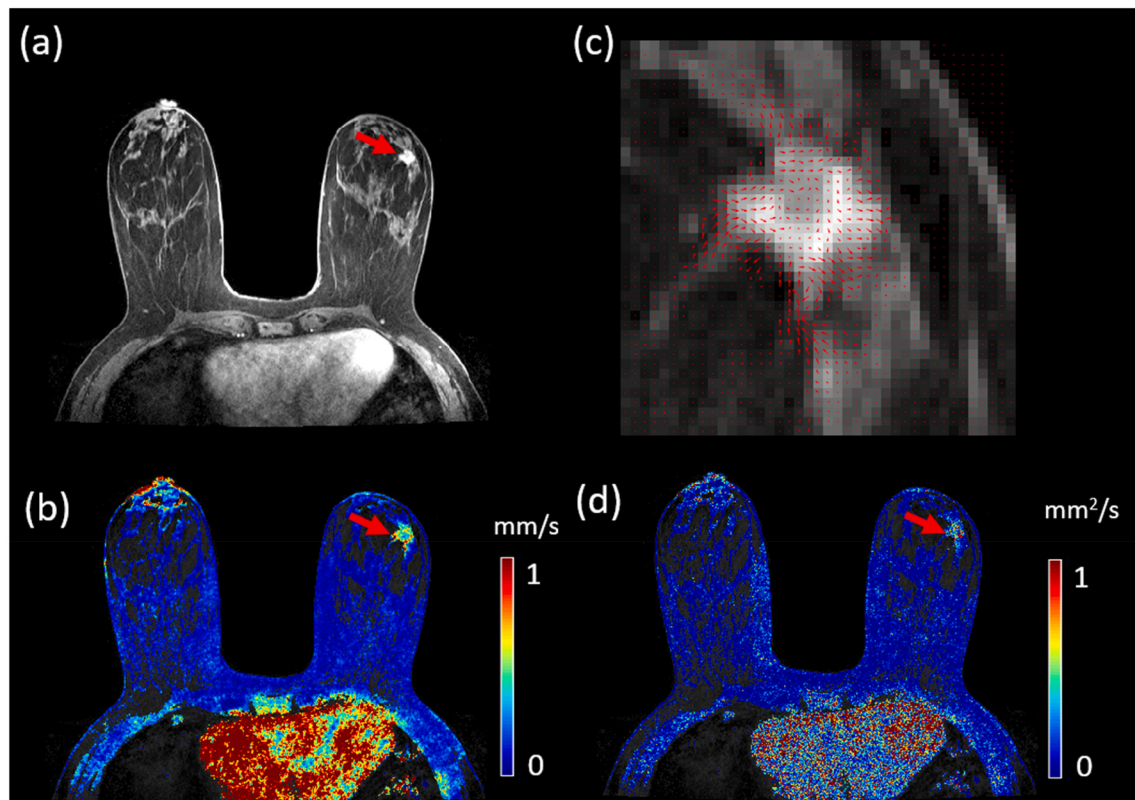


Fig. 1. Breast tumor DCE MRI and QTM velocity in an axial section demonstrating carcinoma in a 70 years old patient with biopsy proven malignant lesion. a) post Gd T1 weighted image showing the tumor (red arrow). b) QTM $|u|$ map, and c) vector field map for the lesion, and d) QTM D map. (For interpretation of the references to colour in this figure legend, the reader is referred to the web version of this article.)

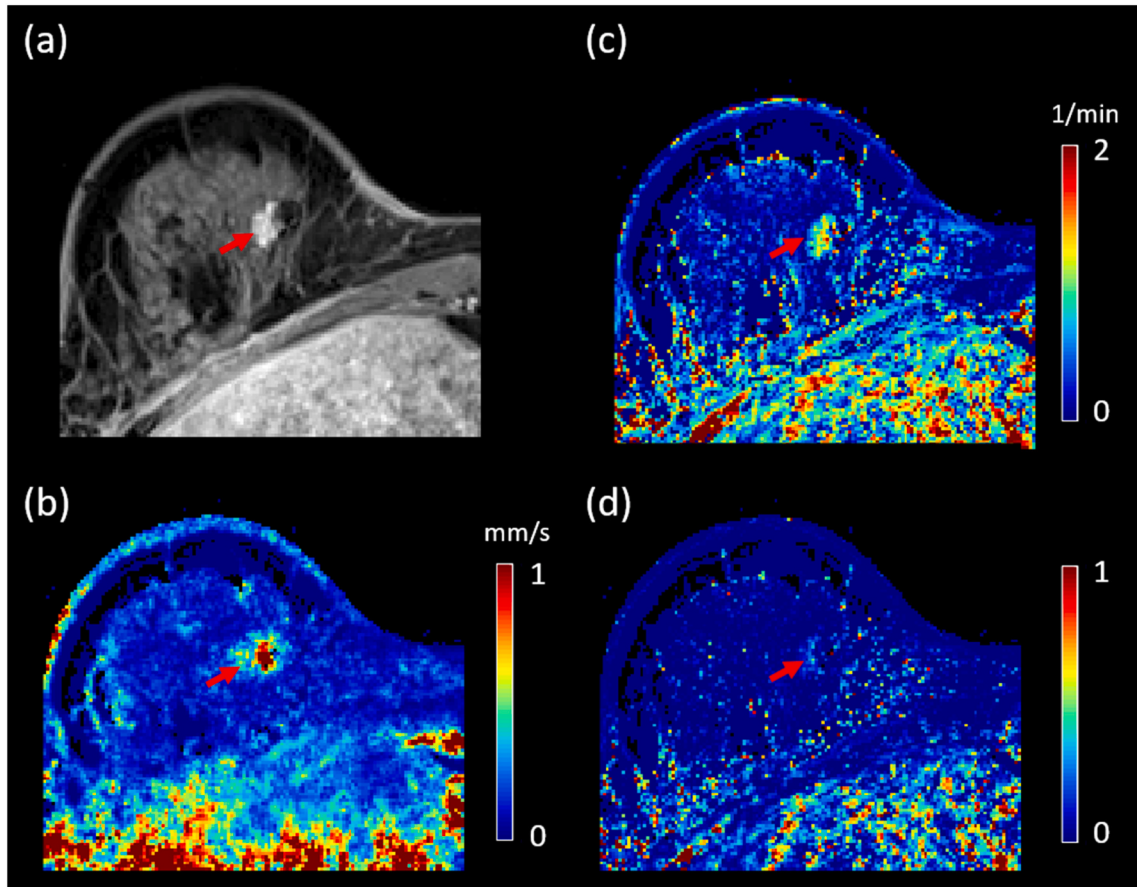


Fig. 2. Comparison of QTM method and kinetics method on a malignant lesion. This is a 53 years old patient with biopsy proven benign lesion. a) post-Gd T1 weighted image, b) QTM $|u|$ map, c) K^{trans} and d) V_e map using internal mammary (IM) AIF.

$$\mathbf{u}, D = \underset{\mathbf{u}, D}{\operatorname{argmin}} \sum_{t=1}^{N_t-1} \|\partial_t c + \nabla \cdot c \mathbf{u} - \nabla \cdot D \nabla c\|_2^2 + \lambda \|\nabla \mathbf{u}\|_1 + \mu \|\nabla D\|_1. \quad (2)$$

In traditional kinetics (extended Tofts' model), the tracer concentration profile is modeled by [2]:

$$\partial_t c(\mathbf{r}, t) = K^{\text{trans}}(\mathbf{r}) \left[c_a(t) - \frac{1}{V_e(\mathbf{r})} c(\mathbf{r}, t) \right], \quad (3)$$

where $c_a(t)$ is the global AIF, K^{trans} is volume transfer constant, $V_e(\mathbf{r})$ is a linear equation system for K^{trans} and $k_{ep} = \frac{K^{\text{trans}}}{V_e}$, but is nonlinear to τ . A voxel wise non-linear least square method is used to solved for kinetic parameters and traveling delay τ of AIF with the regularization parameters $\lambda = \mu = 10^{-3}$ chosen according to the L-curve method [6,21,22]:

$$K^{\text{trans}}, k_{ep}, \tau = \underset{K^{\text{trans}}, k_{ep}, \tau}{\operatorname{argmin}} \sum_{t=1}^{N_t-1} \|\partial_t c - K^{\text{trans}} c_a(t-\tau) + k_{ep} c\|_2^2 + \lambda \|\nabla K^{\text{trans}}\|_1 + \mu \|\nabla k_{ep}\|_1 \quad (4)$$

In traditional semi-quantitative tissue enhancement curve characterization, the tracer concentration in the tumor ROI at each time point is modeled by [23],

$$\Delta S(t) = \frac{S(t) - S(0)}{S(0)} = A(1 - e^{-\alpha t})e^{-\beta t}, \quad (5)$$

where A is the enhancement amplitude, α is the wash in rate and β the wash out rate. The Levenberg–Marquardt algorithm is used to perform the nonlinear curve fitting:

$$A, \alpha, \beta = \underset{A, \alpha, \beta}{\operatorname{argmin}} \sum_{t=1}^{N_t-1} |\Delta S(t) - A(1 - e^{-\alpha t})e^{-\beta t}|_2^2. \quad (6)$$

2.2. Clinical data

The retrospective analysis of DCE-MRI data in this study was approved by the Institutional Review Board and was HIPAA compliant. We enrolled 26 consecutive female patients, who had 1) undergone MRI of the mammary glands for suspicious lesions on mammography/ultrasound, 2) DCE-MRI as part of their routine clinical MRI protocol on a 3 T MRI system (Magnetom Skyra, Siemens), and 3) biopsy. 30 lesions were specified, and for the patients with multiple lesions, the lesion with the largest size was included. Detailed patient and lesion information are shown in Table 1.

All patients were imaged between 06/14/2019 and 01/18/2020 using an 8-channel breast coil to acquire DCE-MRI immediately after the start of contrast injection for 5 phases. The temporal resolution is 15.4 s per frame and the total scan time was 77 s. The gadolinium-based contrast agent (gadobutrol; Bayer Healthcare Pharmaceuticals Inc., Whippany, NJ) was administered at 2 ml/s (dose = 0.1 mmol/kg body weight), followed by 40 ml saline flush at 2 ml/s. The DCE-MRI

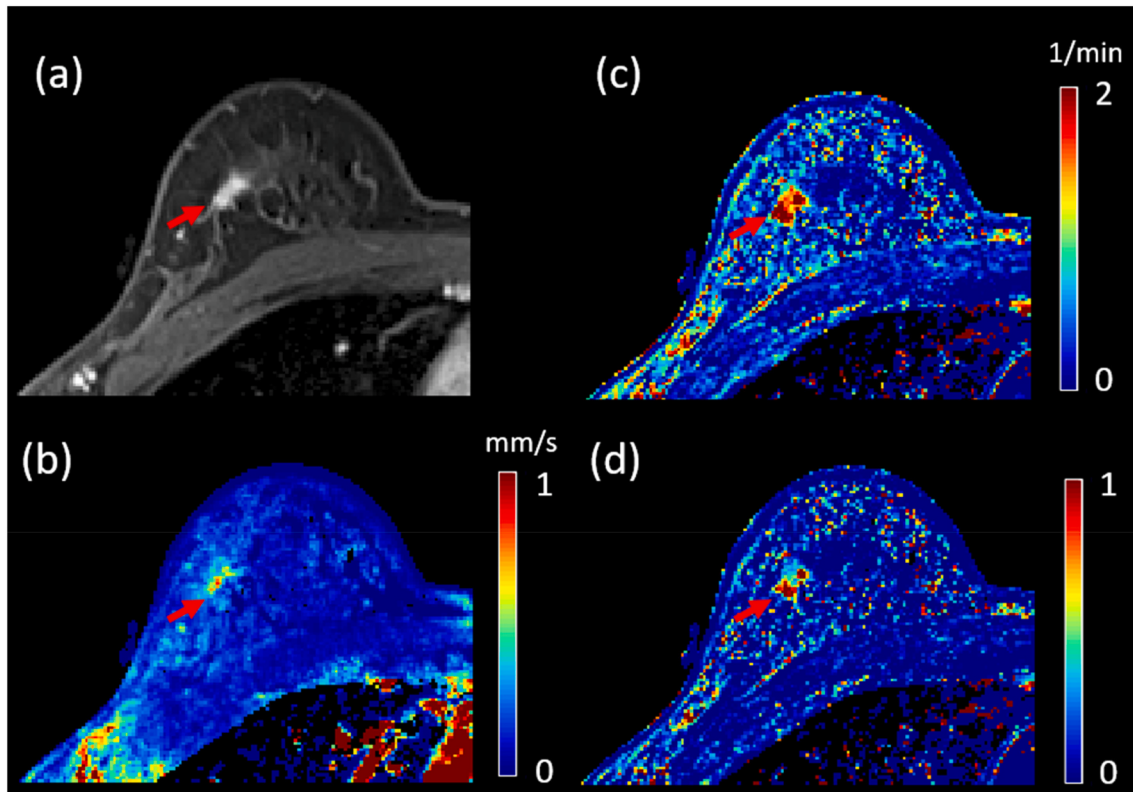


Fig. 3. Comparison of QTM method and kinetics method on a benign lesion. This is a 45 years old patient with biopsy proven malignant lesion. a) post-Gd T1 weighted image, b) QTM $|u|$ map, c) K^{trans} and d) V_e map using internal mammary artery AIF.

acquisition parameters were: TR/TE = 3.95/1.7 msec, flip angle = 10°, in-plane spatial resolution = 0.71 mm, thickness = 1.8 mm, axial orientation [24].

For each case, an experienced radiologist selected an AIF by drawing an ROI on the internal mammary artery. The same radiologist, blinded to the diagnosis, manually segmented regions of interest (ROI) comprised of the whole tumor volume based on the enhanced area in DCE image for analysis. The velocity amplitude $|u|$, diffusion coefficient D , K^{trans} and V_e were averaged over these ROIs.

2.3. Statistical analysis

Using the R Statistical Software (Foundation for Statistical Computing, Vienna, Austria), a Mann-Whitney U test was performed comparing ROI values between benign and malignant tumors for $|u|$, D , K^{trans} , V_e , A , α and β . P -values at or below 0.05 were considered to indicate statistical significance. A receiver operating characteristic curve (ROC) analysis was performed to investigate the diagnostic performance of all parameters for distinguishing between benign and malignant breast tumors. All reconstructions were performed on a computer using an Intel i7-8700K 6-core CPU with 64GB memory.

3. Results

Fig. 1 shows the velocity amplitude and direction obtained by QTM from DCE-MRI images of a malignant breast lesion. The lesion was well visualized on QTM velocity map (Fig. 1b) and diffusion map (Fig. 1d). The QTM velocity vector map (Fig. 1c) showed flow into and out of the lesion. The reconstructed velocity and diffusion coefficient at the lesion ROI were 0.47 ± 0.25 mm/s and 0.48 ± 0.46 mm 2 /s, respectively.

Figs. 2 and 3 illustrate example maps of QTM velocity $|u|$, K^{trans} and V_e for malignant and benign lesions. The two lesions showed similar enhancement on T1 weighted images of DCE MRI (Figs. 2a & 3a). The

benign lesion showed a lower QTM velocity (Fig. 3b) compared to the malignant lesion (Fig. 2b). Corresponding AIFs, tumor ROI enhancement and fitted enhancement curves are shown in Fig. 4.

The diagnostic performances of the QTM, kinetics method and ECC parameters are summarized Table 2 and illustrated in Fig. 5. A statistically significant difference between malignant and benign lesions was found for QTM velocity $|u|$ (0.45 ± 0.15 vs 0.29 ± 0.11 mm/s, $p = 0.0066$), K^{trans} (1.18 ± 0.49 vs 0.74 ± 0.36 /min, $p = 0.0274$). A statistically significant difference was absent in QTM diffusion D (0.30 ± 0.12 vs 0.21 ± 0.09 mm 2 /s, $p = 0.1119$), in kinetics V_e (0.26 ± 0.15 vs 0.19 ± 0.12 , $p = 0.2382$), AIF delay (5.47 ± 3.69 vs 3.75 ± 2.53 s, $p = 0.2184$), and in enhancement A (6.77 ± 5.74 vs 4.09 ± 2.42 , $p = 0.4418$), α (0.03 ± 0.02 vs 0.02 ± 0.01 /s, $p = 0.2592$) and β (0.007 ± 0.006 /s vs 0.006 ± 0.004 /s, $p = 0.9591$).

Among all these parameters, the highest AUC value was achieved with QTM velocity (0.82, 95% confidence level 0.60–0.95) followed by K^{trans} (0.75, 0.51–0.90). Fig. 6 illustrates their ROCs. No improvement in diagnostic accuracy was found by combining $|u|$ and D for QTM (AUC = 0.83, 95% confidence level 0.63–0.95), or combining K^{trans} , V_e and t for kinetics method (AUC = 0.76, 0.51–0.91), or combining A , α and β for ECC (AUC = 0.63, 0.39–0.82) using logistic regression.

4. Discussion

Our results demonstrate that the inversion of the transport equation or quantitative transport mapping (QTM) is feasible for automated processing of DCE-MRI as applied in breast cancer diagnosis. For performance in differentiating benign from malignant tumors, QTM was compared with two traditional methods of breast DCE-MRI post-processing methods: traditional kinetics method and enhancement curve characteristics (ECC). Using biopsy pathology as reference standard, QTM was found to have the highest accuracy (AUC = 0.82), followed by kinetics method (AUC = 0.75) and then ECC (AUC = 0.63).

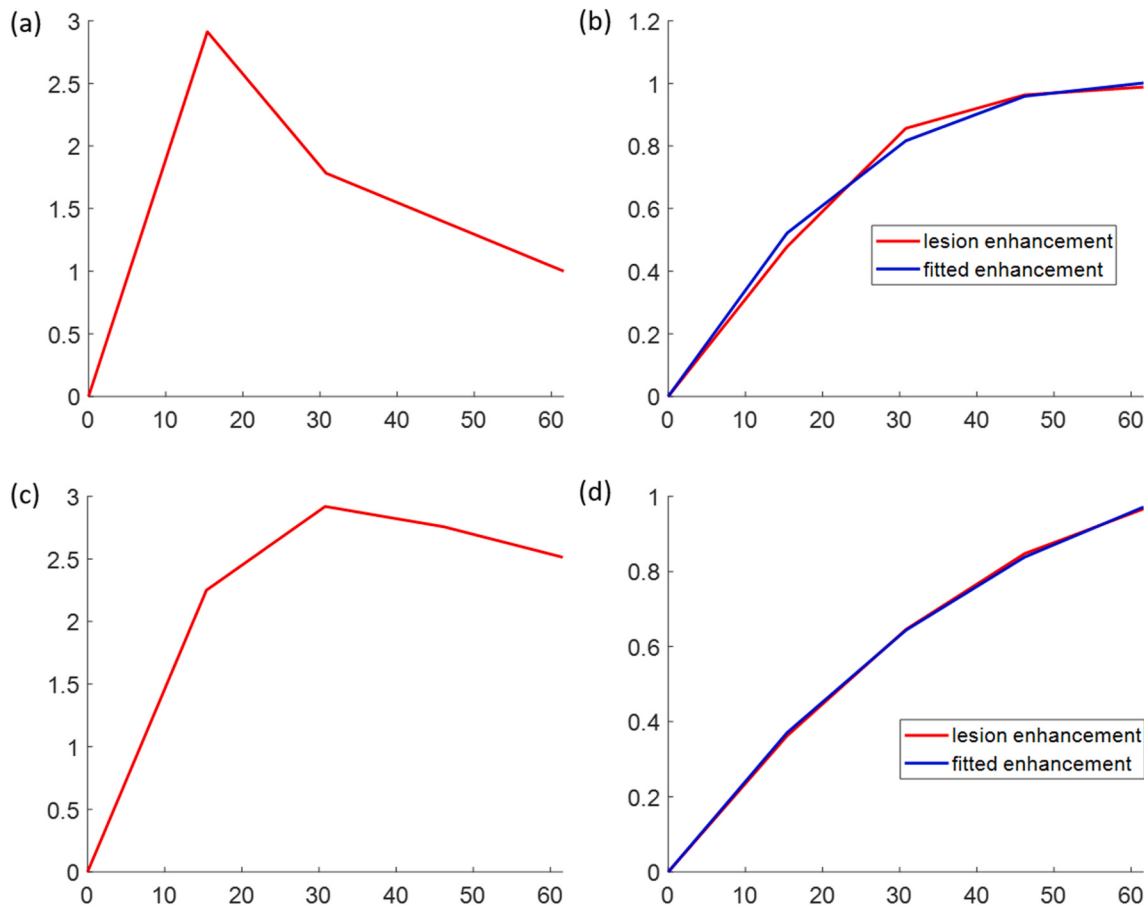


Fig. 4. a) and b) AIF, tumor ROI enhancement curves and fitted enhancement curve for the case in Figs. 2. c) and d) AIF, tumor ROI enhancement curves and fitted enhancement curve for the case in Figs. 3.

Table 2

Diagnostic accuracy of QTM velocity, kinetic modeling parameters and semi-quantitative parameters in distinguishing between benign and malignant breast lesions. 95% confidence level is shown in brackets. The first two columns are the mean value and standard deviation of malignant and benign lesions.

Parameter	Malignant	Benign	AUC	p- value
$ u $	0.45 ± 0.15	0.29 ± 0.11	$0.82 (0.60-0.95)$	0.0066
D	0.30 ± 0.12	0.21 ± 0.09	$0.69 (0.44-0.87)$	0.1119
K^{trans}	1.18 ± 0.49	0.74 ± 0.36	$0.75 (0.51-0.90)$	0.0274
V_e	0.26 ± 0.15	0.19 ± 0.12	$0.64 (0.40-0.83)$	0.2382
τ	5.47 ± 3.69	3.75 ± 2.53	$0.65 (0.40-0.84)$	0.2184
A	6.77 ± 5.74	4.09 ± 2.42	$0.59 (0.33-0.80)$	0.4418
α	0.03 ± 0.02	0.02 ± 0.01	$0.63 (0.42-0.83)$	0.2592
β	0.007 ± 0.006	0.006 ± 0.005	$0.51 (0.27-0.74)$	0.9591

$|u|$: QTM velocity magnitude in mm/s; D : QTM diffusion coefficient in mm^2/s . K^{trans} : kinetic blood flow in 1/min. V_e : kinetic EES volume fraction. τ : AIF delay time in s. A: enhancement amplitude, α : wash-in rate in 1/s, and β : wash-out rate in 1/s.

The accuracy and automation of QTM suggest that QTM has the potential to improve quantitative perfusion postprocessing of DEC-MRI in clinical practice.

The better diagnostic performance of QTM over traditional kinetics method and ECC may be explained by the use of spatial deconvolution in QTM. While all three methods share temporal deconvolution (Eqs. 2, 4 and 6), there is no spatial deconvolution in kinetics method or ECC. QTM uses the spatial divergence of mass flux to model an effective local flow into and out of a voxel, which performs like an effective local AIF. Furthermore, the QTM method using the spatial divergence reflects

spatial features inside tumor and parenchymal enhancement in neighboring tissue that are helpful for tumor classification [25,26]. Therefore, QTM overcomes the problematic use of global AIF in kinetics method. Our clinical data suggests that the velocity output from spatial deconvolution is sensitive to the angiogenic difference between benign and malignant tumors. A voxel-specific AIF delay fitting (Eq. 4) was performed in this study, generating K^{trans} and V_e in the range of values reported in previous studies [27,28]; yet the use of a global AIF profile form suffers from errors associated with dispersion associated with multiplicative arterial supplies to tissue in a voxel.

Another important feature of QTM is full automation in post-processing DCE MRI data. This adds important practical clinical value. Conventional kinetics method typically requires a manual input for an arterial region, which renders the output user dependent. There have been many attempts to automate kinetics method for processing DCE-MRI, including the use of a population-averaged 2-parameter AIF [29] and a blinded estimate of an AIF at each voxel using an 11-parameter model [4]. The population averaged AIF is problematic in clinical applications [10]. The blind deconvolution is yet to be translated into clinical practice, and the AIF distribution in an image volume cannot be fully characterized by 11 parameters in the presence of disease [3,7]. Automated AIF is still being developed using various computer vision methods [30–32] but represents an extra processing step. Currently, AIF selection remains a hurdle for kinetics method, and clinical practices employ descriptive measures instead [14,15].

Tissue perfusion modeling fundamentally requires detailed microvasculature and otherwise is difficult to formulate and validate [20]. Eqs. 1 for QTM and Eq. 3 for kinetics method should be regarded as hypothetical equations expressing linear relationships of tracer voxel

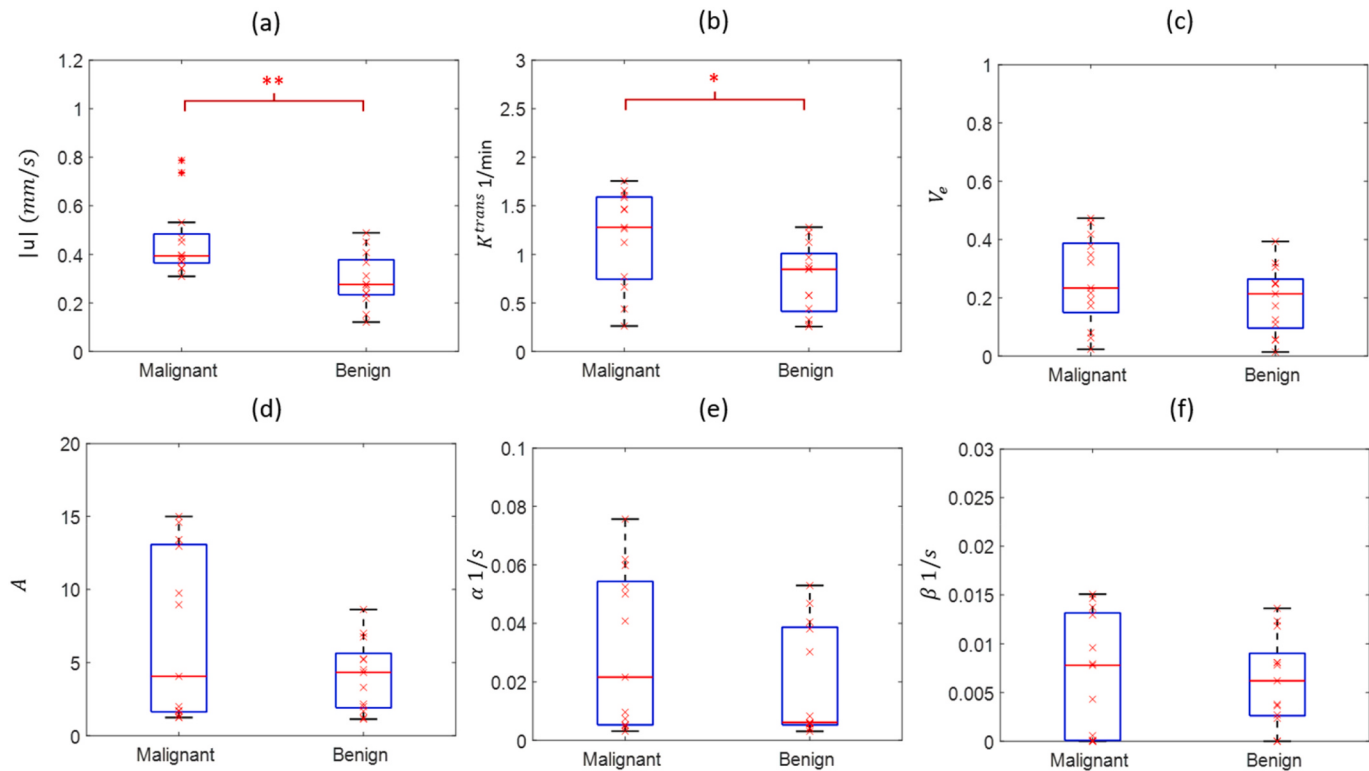


Fig. 5. Differentiating malignant breast lesions from benign breast lesions. a) QTM $|u|$ ($p = 0.0066$), b) K^{trans} ($p = 0.0274$) demonstrating significance difference between malignant and benign lesions. There were no other parameters demonstrating significant difference between malignant and benign lesions.

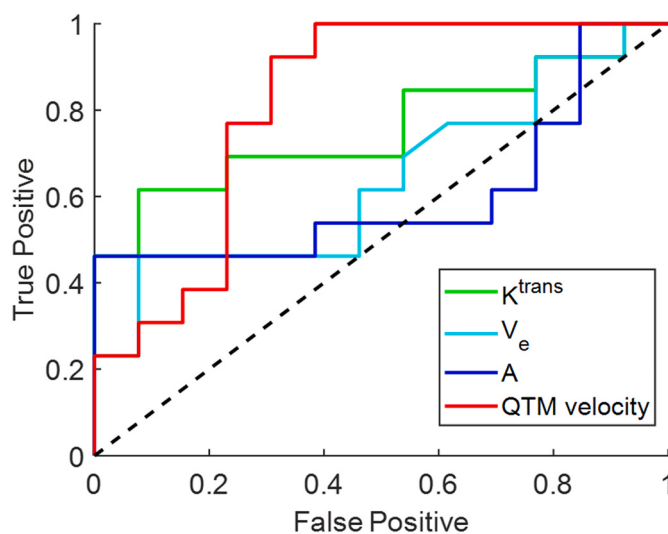


Fig. 6. Receiver operating characteristic curve (ROC) for $|u|$, K^{trans} , V_e and A in differentiating malignant and benign lesions.

concentration in space and time, as they cannot be readily derived from basic laws of physics. Eq. 3 for kinetics method is a symbolical extension from the original use of the Fick principle of mass conservation between blood input and output to an organ [1] to tomographic perfusion with the inherent difficulty of an unmeasurable AIF at each voxel [3]. Similarly, Eq. 1 is also a symbolical extension from the continuity equation of transport equation in continuous space to the voxel level tracer propagation using symbolic mass flux of convection velocity and diffusion [16,33,34]. The symbolical quantities, velocity $u(r)$ and diffusion $D(r)$ in Eq. 3, have now readily-

defined physical meanings and need to be justified according to the physics law of fluid mechanics and tissue microvasculature details in a voxel. When the microvasculature is porous as in certain tumors [35] or tree-like in renal tissue [36], Eq. 1 can be validated by integrating the solution to the continuous transport equations of both mass and momentum fluxes over the detailed microvasculature in each voxel and the velocity u represents an average fluid velocity in a voxel [19,37,38]. Of course, the fluid mechanics validation is straightforward for voxels containing only blood, as explored in x-ray angiographic video [39] and in optical video [40], or for interpreting the velocities (averaged over imaging time) of cardiac chambers in this study. To our knowledge, Eq. 3 for kinetics method has never been validated according to the continuous transport equation of fluid mechanics and tissue microvasculature. Breast tumor microvasculature in a mouse xenograft is available for computational blood flow predictions [41], which may be extended to human breast tumor to validate Eqs. 1 and 3 in a future investigation [42].

Instead of validating Eq. 1 for QTM and Eq. 3 for kinetics method according to the fundamental transport equation of fluid mechanics and tissue microvasculature, clinical applications can be used to justify the use of these equations in modeling DCE-MRI. In fact, DCE-MRI literature is largely based on using pathology-proven tumor malignancy to justify the use of Eq. 3 in kinetics method [43,44] and Eq. 5 for ECC [45]. Accordingly, pathology from biopsy was used in this study. The results show that QTM is more accurate than kinetics method and ECC for differentiating malignant from benign tumors in breast DCE-MRI.

The inversion of linear Eq. 1 is determined by the condition of its system matrix, which is poor and requires denoising regularization in postprocessing noisy DCE-MRI data [20]. The diffusion term in Eq. 1 seems unimportant for DCE-MRI postprocessing, which requires further investigation. The lack of accuracy improvement by logistic regression of combining parameters may be because of a small sample size and the correlation among parameters.

This preliminary work on QTM has several other limitations to be

addressed in future work. 1) The whole voxel is treated as a single compartment. A multi-compartment model can be employed to resolve velocities and kinetics in vessel and other compartments [16]. 2) Numerical simulations with detailed vasculature model [42] and computational fluid dynamics and imaging experiments in 3D printed phantoms with known ground truth should be developed to validate all perfusion quantification methods including QTM and kinetics method. This would require future efforts to improve upon recent attempts with simple sphere or tubes in simulation and experiments [46,47]. 3) There may be motion during DCE MRI acquisition, and navigator method may be used for motion compensation [48–51]. 4) Gd concentration was approximated as relative signal enhancement, which may contain errors. These errors can be corrected using quantitative susceptibility mapping [52,53], which can provide accurate estimation Gd concentration [54–56]. 5) The temporal resolution was 15 s per timeframe, which is the current clinical standard [24] but may be limiting for evaluating time derivatives for QTM and traditional kinetics, for defining AIF in traditional kinetic methods, for estimating parameters in semi quantitative method. Fast imaging can improve the temporal resolution [57]. However, intravenous injection with cardiopulmonary mixing may fundamentally smooth tracer concentration temporal variation to 10s scale. 6) Only 5 data points were acquired for each subject. More data points may improve the robustness of inversion process for QTM and traditional kinetics, and it may also benefit the parameter estimation in semi-quantitative methods [27,58]. Overcoming these limitations has the potential to further improve the accuracy of QTM method and make QTM useful for other clinical situations.

In summary, QTM with spacetime deconvolution is feasible for determining a velocity from time resolved imaging of tracer transport in tissue. The QTM method automatically generates a velocity vector map from DCE-MRI data, without requiring an AIF. Compared to traditional kinetics method and enhancement curve characteristics, QTM velocity had higher diagnostic accuracy in distinguishing benign from malignant breast lesions.

Author statement

Qihao Zhang: Data curation; Formal analysis; Investigation; Methodology; Software; Validation; Visualization; Roles/Writing - original draft; Writing - review & editing.

Pascal Spincemaille: Conceptualization; Data curation; Formal analysis; Methodology; Validation; Visualization; Writing - review & editing.

Michele Drotman: Data curation; Formal analysis; Investigation; Resources; Writing - review & editing.

Christine Chen: Data curation; Formal analysis; Investigation; Resources; Writing - review & editing.

Sarah Eskreis-Winkler: Data curation; Formal analysis; Investigation; Resources; Writing - review & editing.

Weiyuan Huang: Data curation; Formal analysis; Investigation; Resources; Writing - review & editing.

Liangdong Zhou: Conceptualization; Formal analysis; Investigation; Methodology; Validation; Visualization; Writing - review & editing.

John Morgan: Conceptualization; Formal analysis; Investigation; Methodology; Validation; Visualization; Writing - review & editing.

Thanh D. Nguyen: Conceptualization; Data curation; Formal analysis; Methodology; Validation; Visualization; Writing - review & editing.

Martin R. Prince: Data curation; Project administration; Writing - review & editing.

Yi Wang: Conceptualization; Funding acquisition; Methodology; Project administration; Resources; Supervision; Writing - review & editing.

References

- [1] Kety SS. The theory and applications of the exchange of inert gas at the lungs and tissues. *Pharmacol. Rev.* 1951;3(1):1–41.
- [2] Tofts PS, Brix G, Buckley DL, Eveloch JL, Henderson E, Knopp MV, et al. Estimating kinetic parameters from dynamic contrast-enhanced T1-weighted MRI of a diffusible tracer: standardized quantities and symbols. *J. Magn. Reson. Imaging* 1999;10(3):223–32.
- [3] Calamante F. Arterial input function in perfusion MRI: a comprehensive review. *Prog. Nucl. Magn. Spectrosc.* 2013;74:1–32.
- [4] Fluckiger JU, Schabel MC, DiBella EV. Model-based blind estimation of kinetic parameters in dynamic contrast enhanced (DCE)-MRI. *Magn. Reson. Med.* 2009;62(6):1477–86.
- [5] Chouhan MD, Bainbridge A, Atkinson D, Punwani S, Mookerjee RP, Lythgoe MF, et al. Estimation of contrast agent bolus arrival delays for improved reproducibility of liver DCE MRI. *Phys. Med. Biol.* 2016;61(19):6905–18.
- [6] Jafar R, Chhabra S, Prince MR, Wang Y, Spincemaille P. Vastly accelerated linear least-squares fitting with numerical optimization for dual-input delay-compensated quantitative liver perfusion mapping. *Magn. Reson. Med.* 2018;79(4):2415–21.
- [7] Calamante F. Bolus dispersion issues related to the quantification of perfusion MRI data. *J. Magn. Reson. Imaging* 2005;22(6):718–22.
- [8] Keil VC, Madler B, Gieseke J, Timmers R, Hattingen E, Schild HH, et al. Effects of arterial input function selection on kinetic parameters in brain dynamic contrast-enhanced MRI. *Magn. Reson. Imaging* 2017;40:83–90.
- [9] Heye T, Davenport MS, Horvath JJ, Feuerlein S, Breault SR, Bashir MR, et al. Reproducibility of dynamic contrast-enhanced MR imaging. Part I. perfusion characteristics in the female pelvis by using multiple computer-aided diagnosis perfusion analysis solutions. *Radiology* 2013;266(3):801–11.
- [10] Woolf DK, Taylor NJ, Makris A, Tunari N, Collins DJ, Li SP, et al. Arterial input functions in dynamic contrast-enhanced magnetic resonance imaging: which model performs best when assessing breast cancer response? *Br. J. Radiol.* 2016;89(1063):20150961.
- [11] Kudo K, Sasaki M, Yamada K, Momoshima S, Utsunomiya H, Shirato H, et al. Differences in CT perfusion maps generated by different commercial software: quantitative analysis by using identical source data of acute stroke patients. *Radiology* 2010;254(1):200–9.
- [12] Woolf DK, Taylor NJ, Makris A, Tunari N, Collins DJ, Li SP, et al. Arterial input functions in dynamic contrast-enhanced magnetic resonance imaging: which model performs best when assessing breast cancer response? *Br. J. Radiol.* 2016;89(1063):20150961.
- [13] Chen J, Yao J, Thomasson D. Automatic determination of arterial input function for dynamic contrast enhanced MRI in tumor assessment. In: International Conference on Medical Image Computing and Computer-Assisted Intervention. Springer; 2008. p. 594–601.
- [14] D'Orsi CJ, Sickles EA, Mendelson EB, Morris EA, et al. ACR BI-RADS atlas: Breast imaging reporting and data system. American College of Radiology: Reston, VA; 2013.
- [15] Turkbey B, Rosenkrantz AB, Haider MA, Padhani AR, Villeirs G, Macura KJ, et al. Prostate imaging reporting and data system version 2.1: 2019 update of prostate imaging reporting and data system version 2. *Eur. Urol.* 2019;76(3):340–51.
- [16] Sourbron S. A tracer-kinetic field theory for medical imaging. *IEEE Trans. Med. Imaging* 2014;33(4):935–46.
- [17] Spincemaille P, Zhang Q, Nguyen TD, Wang Y. Vector field perfusion imaging. ISMRM Annual Meeting Hawaii 2017;3793.
- [18] Zhou L, Spincemaille P, Zhang Q, Nguyen T, Doyeux V, Lorthois S, et al. Vector Field Perfusion Imaging: A Validation Study by Using Multiphysics Model1870. Paris, France: ISMRM Annual Meeting; 2018.
- [19] Zhou L, Zhang Q, Spincemaille P, Nguyen T, Wang Y. Quantitative transport mapping (QTM) of the kidney using a microvascular network approximation. Annual Meeting of ISMRM Montreal 2019;703.
- [20] Zhou L, Zhang Q, Spincemaille P, Nguyen TD, Morgan J, Dai W, et al. Quantitative transport mapping (QTM) of the kidney with an approximate microvascular network. *Magn. Reson. Med.* 2021;85(4):2247–62.
- [21] Murase K. Efficient method for calculating kinetic parameters using T1-weighted dynamic contrast-enhanced magnetic resonance imaging. *Magn. Reson. Med.* 2004;51(4):858–62.
- [22] Kallehauge JF, Sourbron S, Irving B, Tanderup K, Schnabel JA, Chappell MA. Comparison of linear and nonlinear implementation of the compartmental tissue uptake model for dynamic contrast-enhanced MRI. *Magn. Reson. Med.* 2017;77(6):2414–23.
- [23] Jansen SA, Fan X, Karczmar GS, Abe H, Schmidt RA, Newstead GM. Differentiation between benign and malignant breast lesions detected by bilateral dynamic contrast-enhanced MRI: a sensitivity and specificity study. *Magn. Reson. Med.* 2008;59(4):747–54.
- [24] El Khouri RH, Macura KJ, Jacobs MA, Khalil TH, Kamel IR, Dwyer A, et al. Dynamic contrast-enhanced MRI of the breast: quantitative method for kinetic curve type assessment. *AJR Am. J. Roentgenol.* 2009;193(4):W295–300.
- [25] Chen J-H, Yu H, Lin M, Mehta RS, Su M-Y. Background parenchymal enhancement in the contralateral normal breast of patients undergoing neoadjuvant chemotherapy measured by DCE-MRI. *Magn. Reson. Imaging* 2013;31(9):1465–71.
- [26] Yin X-X, Hadjiloucas S, Chen J-H, Zhang Y, Wu J-L, Su M-Y. Tensor based multichannel reconstruction for breast tumours identification from DCE-MRIs. *PLoS One* 2017;12(3):e0172111.
- [27] Sorace AG, Partridge SC, Li X, Virostko J, Barnes SL, Hippe DS, et al. Distinguishing benign and malignant breast tumors: preliminary comparison of kinetic modeling approaches using multi-institutional dynamic contrast-enhanced MRI data from the

- international breast MR consortium 6883 trial. *Journal of Medical Imaging* 2018;5(1):011019.
- [28] Amarnath J, Sangeeta T, Mehta SB. Role of quantitative pharmacokinetic parameter (transfer constant: Ktrans) in the characterization of breast lesions on MRI. *Indian J. Radiol. & Imag.* 2013;23(1):19.
- [29] Parker GJ, Roberts C, Macdonald A, Buonaccorsi GA, Cheung S, Buckley DL, et al. Experimentally-derived functional form for a population-averaged high-temporal-resolution arterial input function for dynamic contrast-enhanced MRI. *Magn. Reson. Med.* 2006;56(5):993–1000.
- [30] Fan S, Bian Y, Wang E, Kang Y, Wang DJJ, Yang Q, et al. An automatic estimation of arterial input function based on multi-stream 3D CNN. *Front Neuroinform* 2019;13:49.
- [31] Yin J, Yang J, Guo Q. Automatic determination of the arterial input function in dynamic susceptibility contrast MRI: comparison of different reproducible clustering algorithms. *Neuroradiology* 2015;57(5):535–43.
- [32] Chen J, Yao J, Thomasson D. Automatic determination of arterial input function for dynamic contrast enhanced MRI in tumor assessment. *Med Image Comput Comput Assist Interv* 2008;11(Pt 1):594–601.
- [33] Pellerin M, Yankeelov TE, Lepage M. Incorporating contrast agent diffusion into the analysis of DCE-MRI data. *Magn. Reson. Med.* 2007;58(6):1124–34.
- [34] Koh TS, Hartono S, Thng CH, Lim TK, Martarello L, Ng QS. In vivo measurement of gadolinium diffusivity by dynamic contrast-enhanced MRI: a preclinical study of human xenografts. *Magn. Reson. Med.* 2013;69(1):269–76.
- [35] Farnsworth RH, Lackmann M, Achen MG, Stack SA. Vascular remodeling in cancer. *Oncogene* 2014;33(27):3496–505.
- [36] Nordsletten DA, Blackett S, Bentley MD, Ritman EL, Smith NP. Structural morphology of renal vasculature. *Am. J. Physiol. Heart Circ. Physiol.* 2006;291(1):H296–309.
- [37] Cookson AN, Lee J, Michler C, Chabiniok R, Hyde E, Nordsletten D, et al. A spatially-distributed computational model to quantify behaviour of contrast agents in MR perfusion imaging. *Med. Image Anal.* 2014;18(7):1200–16.
- [38] Bear J. Dynamics of fluids in porous media. Courier Corporation; 2013.
- [39] Shpilfoygel SD, Close RA, Valentino DJ, Duckwiler GR. X-ray videodensitometric methods for blood flow and velocity measurement: a critical review of literature. *Med. Phys.* 2000;27(9):2008–23.
- [40] Liu T, Shen L. Fluid flow and optical flow. *J. Fluid Mech.* 2008;614:253–91.
- [41] Stamatelos SK, Kim E, Pathak AP, Popel AS. A bioimage informatics based reconstruction of breast tumor microvasculature with computational blood flow predictions. *Microvasc. Res.* 2014;91:8–21.
- [42] Wu C, Hormuth DA, Oliver TA, Pineda F, Lorenzo G, Karczmar GS, et al. Patient-Specific Characterization of Breast Cancer Hemodynamics Using Image-Guided Computational Fluid Dynamics. *IEEE Trans Med Imaging*; 2020.
- [43] Kim SG, Freed M, Leite APK, Zhang J, Seuss C, Moy L. Separation of benign and malignant breast lesions using dynamic contrast enhanced MRI in a biopsy cohort. *J. Magn. Reson. Imaging* 2017;45(5):1385–93.
- [44] Wu C, Pineda F, Hormuth 2nd DA, Karczmar GS, Yankeelov TE. Quantitative analysis of vascular properties derived from ultrafast DCE-MRI to discriminate malignant and benign breast tumors. *Magn. Reson. Med.* 2019;81(3):2147–60.
- [45] Jansen SA, Fan X, Karczmar GS, Abe H, Schmidt RA, Newstead GM. Differentiation between benign and malignant breast lesions detected by bilateral dynamic contrast-enhanced MRI: a sensitivity and specificity study. *Magn. Reson. Med.* 2008;59(4):747–54.
- [46] Hariharan P, Freed M, Myers MR. Use of computational fluid dynamics in the design of dynamic contrast enhanced imaging phantoms. *Phys. Med. Biol.* 2013;58(18):6369–91.
- [47] Kim H, Mousa M, Schexnailder P, Hergenrother R, Bolding M, Ntsikoussalabongui B, et al. Portable perfusion phantom for quantitative DCE-MRI of the abdomen. *Med. Phys.* 2017;44(10):5198–209.
- [48] Wang Y, Grist TM, Korosec FR, Christy PS, Alley MT, Polzin JA, et al. Respiratory blur in 3D coronary MR imaging. *Magn. Reson. Med.* 1995;33(4):541–8.
- [49] Wang Y, Rossman PJ, Grimm RC, Wilman AH, Riederer SJ, Ehman RL. 3D MR angiography of pulmonary arteries using real-time navigator gating and magnetization preparation. *Magn. Reson. Med.* 1996;36(4):579–87.
- [50] Wang Y, Ehman RL. Retrospective adaptive motion correction for navigator-gated 3D coronary MR angiography. *J. Magn. Reson. Imaging* 2000;11(2):208–14.
- [51] Lin W, Guo J, Rosen MA, Song HK. Respiratory motion-compensated radial dynamic contrast-enhanced (DCE)-MRI of chest and abdominal lesions. *Magn. Reson. Med.* 2008;60(5):1135–46.
- [52] de Rochefort L, Liu T, Kressler B, Liu J, Spincemaille P, Lebon V, et al. Quantitative susceptibility map reconstruction from MR phase data using bayesian regularization: validation and application to brain imaging. *Magn. Reson. Med.* 2010;63(1):194–206.
- [53] Deh K, Nguyen TD, Eskreis-Winkler S, Prince MR, Spincemaille P, Gauthier S, et al. Reproducibility of quantitative susceptibility mapping in the brain at two field strengths from two vendors. *J. Magn. Reson. Imaging* 2015;42(6):1592–600.
- [54] de Rochefort L, Nguyen T, Brown R, Spincemaille P, Choi G, Weinsaft J, et al. In vivo quantification of contrast agent concentration using the induced magnetic field for time-resolved arterial input function measurement with MRI. *Med. Phys.* 2008;35(12):5328–39.
- [55] Bonekamp D, Barker PB, Leigh R, van Zijl PC, Li X. Susceptibility-based analysis of dynamic gadolinium bolus perfusion MRI. *Magn. Reson. Med.* 2015;73(2):544–54.
- [56] Xu B, Spincemaille P, Liu T, Prince MR, Dutruel S, Gupta A, et al. Quantification of cerebral perfusion using dynamic quantitative susceptibility mapping. *Magn. Reson. Med.* 2015;73(4):1540–8.
- [57] Xu B, Spincemaille P, Chen G, Agrawal M, Nguyen TD, Prince MR, et al. Fast 3D contrast enhanced MRI of the liver using temporal resolution acceleration with constrained evolution reconstruction. *Magn. Reson. Med.* 2013;69(2):370–81.
- [58] Cheng L, Li X. Breast magnetic resonance imaging: kinetic curve assessment. *Gland Surg* 2013;2(1):50.